Improvements on the Incremental Conductance MPPT Method Applied to a PV String with Single-Phase to Three-Phase Converter for Rural Grid Applications

Luís Fernando Corrêa MONTEIRO, Cleiton Magalhães FREITAS, Maria Dias BELLAR
Rio de Janeiro State University, 20550-900, Rio de Janeiro-RJ, Brazil
lmonteiro@uerj.br

***Abstract*—A power electronic interface that integrates a photovoltaic string with a single-phase grid to feed a three-phase induction motor, while driving a fan-type load, is presented. The interface is composed of a single-phase active rectifier and a three-phase inverter with output transformer, wherein the Photovoltaic (PV) string is straightly connected to the DC-link, avoiding the use of additional converter for maximum power point tracking, commonly seen in previous works. However, in this system configuration, disturbances at the DC-link may occur due to increments and decrements of load active power, with consequent low-frequency oscillations at the AC grid side of the active rectifier. Therefore, a modified Incremental Conductance based algorithm is proposed, with which low-frequency oscillations around the maximum power point are minimized even under disturbances at the DC-link. Moreover, the overall system energy management, composed of control algorithms, that integrates maximum power point identification, DC-link voltage regulation, motor speed controller and power quality at the input AC mains, is also proposed. Simulation results are provided to evaluate the system effectiveness under AC mains with voltage sag occurrence, load transient and steady-state conditions at different solar irradiance levels.**

***Index Terms*—rural areas, static power converters, power system dynamics, solar power generation, iterative algorithms.**

I. INTRODUCTION

The large scale of global energy demands for promoting industrialization and improving quality of life has increasingly damaged environmental resources worldwide [1]. In addition to that, recent studies have indicated that renewable energy sources are technically and economically feasible to meet all the global energy needs [2], which may serve as encouragement for more research and development of renewable energy based equipment. Encompassed by this course of events, power electronic converters have played the key role as the enabling technology for changing paradigms from centralized generation systems with long transmission lines towards distributed generation (DG) systems [3].

The DG concept empowers the integration of different kinds of renewable energy sources and storage systems, and existent conventional sources as well, to supply stand-alone [4] or grid-connected loads [5]. Furthermore, it provides the means of using on-site energy resources minimizing or even eliminating transmission and distribution costs, which is crucial to reduce obstacles for rural or remote areas electrification and to encourage sustainable business development [6].

Different power architectures and converter topologies have been proposed to integrate renewable sources and energy storage systems with the purpose of forming up DG utility grids [7-8]. Among these, two prominent technologies have usually been applied to different kinds of distributed energy systems. One employs a DC-DC converter to interface a renewable source, or an energy storage device, with a DC-link, in order to compose DC-coupled, AC-coupled, or even mixed structures [8]. Particularly in [8] the authors used a Scott transformer for single-phase to three-phase conversion, and in [9] Dual Active Bridge (DAB) converters were applied for connecting solar photovoltaic (PV) panels and battery to a DC micro-grid. With the other power architecture, the renewable source is directly connected to the DC-link of an inverter, whose output terminals may or may not be hooked up to a conventional low -or high-frequency transformer [7].

One typical scenario for considering this technology is the improvement of power system reliability, especially at weak power grids. In Brazil, for example, there is a common sense so far that single-phase circuits for rural grids have been adequate to supply the existing loads in rural areas [10]. Essentially, these single-phase circuits comprehend single-phase with neutral and Single-Wire Earth Return (SWER).

It is also important to emphasize that SWER based grids is very prone to voltage sag occurrences, which characterizes a weak power grid demanding power quality improvements. These functional and operational aspects added to the limited provision of electricity services in country areas, have motivated several works on single-phase to three-phase power electronic systems meant for rural applications [11-13].

In [11], a two-level three-leg three-phase inverter was coupled to a single-phase power source and a three-phase load. In that work, the inverter connection resembled that of a shunt active power filter, having the single-phase source parallel connected to one load phase and to one inverter phase, which drew sinusoidal current from the mains at close to unity power factor. Moreover, a solar photovoltaic (PV) panel was applied to the inverter DC-link, on which it is apparent that a DC-DC converter was employed to perform maximum power point tracking (MPPT).

Digital Object Identifier 10.4316/AECE.2019.01009

Further developments on such single-phase to three-phase system for DG applications were presented in [12], wherein a two-level four-leg power converter had been proposed as an alternative to the conventional five-leg full-bridge converter [13].

Contrastively in [14] an energy generation system based on a PV string straightly connected to the DC-link of a back-to-back converter, consisted of a conventional five-leg full-bridge converter for feeding an induction motor, was proposed. Unlike other works, an extra DC-DC converter to perform MPPT was not needed, since the front-end rectifier executed active input current wave shaping for power factor correction and MPPT as well. Hence, hardware reduction was the main positive aspect.

Furthermore, a modified Gradient Descent (GD) based MPPT was proposed [14] and its performance was compared to that of Perturb and Observe (P&O) method. Although both algorithms could correctly regulate the DC-link voltage for MPP operation, low-frequency disturbances at the rectifier grid-side were verified. Those oscillations may cause malfunction of equipment connected to the Point of Common Coupling (PCC). On top of that, tracking execution quality was dependent on the irradiance variation level.

Therefore, the present article is a further development to that work. In this case, a single-phase to three-phase system, based on the conventional five-leg full-bridge converter with output transformer, for integrating a solar PV string, to feed an induction motor of 10 kW type while driving a fan-type load, is described in detail. A modified Incremental Conductance (InC) based MPPT method to minimize eventual oscillations around the MPP likewise in [14], which may also occur with classical InC technique, is proposed, and this constitutes the first contribution of this paper. Moreover, the proposed MPPT algorithm assures satisfactory dynamics during irradiance variations and provides immunity against possible load transients since, during these disturbances, it keeps the PV string producing its actual MPP. Furthermore, the system energy management is accomplished by the control algorithms that integrates MPP identification, DC-link voltage regulation, motor speed controller and single-phase input current wave shaping with low total harmonic distortion (THD%) and in phase with the AC mains. Such energy management differs from earlier referred works and that corresponds to the second contribution of this paper.

Thus, the present text is aimed to: *i*) describe the design guidelines for specifying the solar PV string and power converters that compose the single-phase to three-phase system; *ii*) explain the control algorithms; *iii*) evaluate the effectiveness of the proposed MPPT algorithm and overall energy management performance, under irradiance and load variations, and single-phase input voltage sag occurrence, by means of simulation results; *iv*) show economic feasibility study, with the purpose of assessing costs, time period and energy payback obtained with the proposed generation system.

II. General System Description

In Fig. 1 the energy system composed of solar PV panels and grid-connected full-controlled five-leg single-phase to three-phase converter supplying an induction motor is illustrated with more details. The system parameters are the following: *i*) single-phase grid voltage at 127 V, 60 Hz; *ii*) grid characteristic inductance (L_S) is 500 µH, which yields a weak power grid with a short-circuit power equal to 10 p.u.; *iii*) induction motor is rated at 460 V, 60 Hz, 10 kW and 1760 rpm; output step-up three-phase transformer of delta-delta type rated at 220 V//460 V, 25 kVA. The use of this transformer is asserted by the inverter output voltage which is set up to 220 V (line voltages).

The single-diode model with shunt and series resistors, to implement each solar PV cell, was adopted for modelling one solar PV panel, wherein commercial parameters of STP255S-20/WD manufactured by Suntech were used. The resultant characteristic curves, for different irradiation values at 25° Celsius, are shown in Fig. 2. Finally, the PV string consists of 17 identical solar panels, with each characteristic curve of them as displayed in Fig. 2.

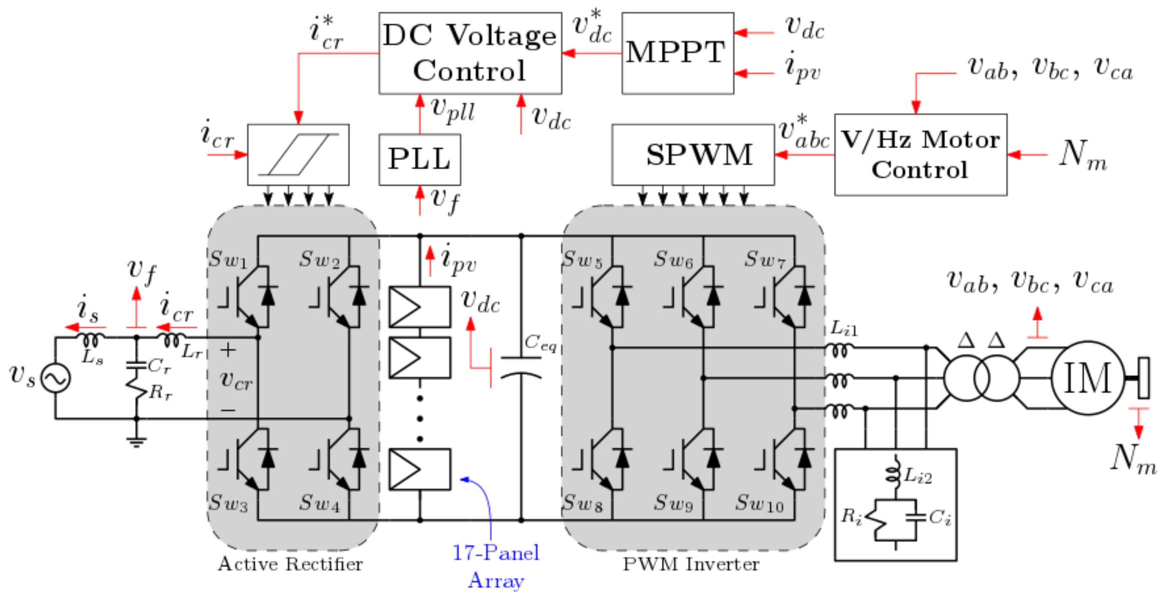

Figure 1. General block diagram of the grid-tied PV generation system

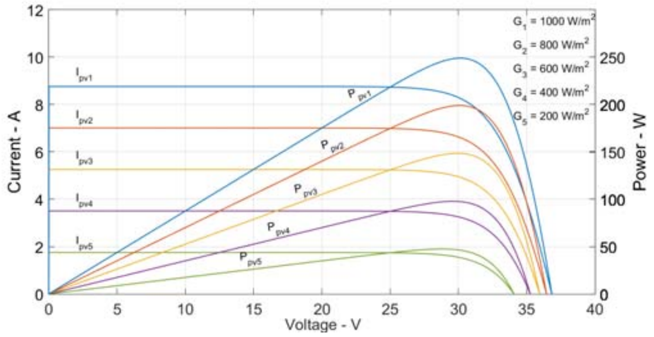

Figure 2. Current Ipv x Voltage and Power (Ppv) x Voltage characteristic curves of the solar PV panel, where G is the solar irradiance, at Standard Test Conditions (STC)

The capacitor bank, at the rectifier DC side, is calculated by considering the second harmonic component (2ω) of the grid angular frequency (ω) only. If one takes the AC side power into account, expressed as average power added to the oscillating power at angular frequency 2ω, and makes it equal to the power at the DC side, it is possible to determine the capacitor bank value as follows:

$$C_{eq} = \frac{V_S\, I_S}{2\omega \Delta v_{DC}\, V_{DC}}\ ; \qquad (1)$$

where V_S and I_S are the peak values of the grid voltage and current respectively; Δv_{dc} is the voltage ripple; ω is the grid angular frequency in rad/s; and V_{DC} is the average DC-link voltage. A 9.4 mF capacitance, C_{eq}, is obtained by making Δv_{dc} 2% of V_{DC}, considering V_{DC} equal to 500 V. This V_{DC} value is assumed by taking into account the fact that, although the DC-link changes dynamically along the day, averagely its value is 500 V as illustrated in the simulation results (Section 4).

The switching method to the active filter corresponds to the current control technique supported on the periodic sampling [15]. This technique leads to a variable switching frequency and, in this work it was limited in a range from 10 kHz to 20 kHz (half of the sampling frequency). To the PWM inverter the switching technique corresponds to the sinusoidal pulse width modulation (SPWM) with fixed frequency at 10 kHz. Feedback loops to control the output fundamental voltage and the mechanical frequency of the motor, by following the Volts/Hz strategy, were also employed. Further aspects of these feedback loops are exploited in Section III.

Low-pass filters were designed as a low-impedance path to the high-frequency harmonic components present in the produced voltages and currents by the active rectifier and PWM converter. To the active rectifier, the low-pass filter is comprehended by a 4 mH filter inductor (L_r) together with a 2.5 Ω resistor (R_r) and a 12.6 μF capacitor (C_r). To the PWM inverter the low-pass filter comprises a 1.0 mH filter inductor (L_{i1}) together with a 500 Ω resistor (R_i), 1.68 μF capacitor (C_i) and another 150 μH inductor (L_{i2}).

III. Control Algorithms

In this section, the control algorithms pertaining the active rectifier, PWM inverter, MPPT and motor drive, are explained. The first aspect to consider for the sake of DC-link controllability is that its value must be higher than the single-phase grid peak voltage, since the active rectifier is a current-controlled voltage source. Secondly, the PV string is specified for voltages not higher than 600 V. Thus, the DC-link voltage is configured to be between 450 V and 600 V. This constraint was necessary since there is no boost stage connecting the PV array to the DC-link.

A. Active Rectifier

The control algorithms of the active rectifier (Fig. 1) consist of the DC-link voltage controller, being the reference value determined by the MPPT algorithm and, further, a switching technique modulates the reference current of the active rectifier, i_{cr}*. This reference current was obtained through a PI controller as follows:

$$\begin{cases} e_{dc}[k] = v_{dc}^*[k] - v_{dc}[k] \\ acum_{dc}[k] = acum_{dc}[k-1] + e_{dc}[k] \\ i_{cr}^*[k] = v_{pll}[k]\cdot\{(k_{p\_dc}\cdot e_{dc}[k]) + (k_{i\_dc}\cdot acum_{dc}[k])\} \end{cases} ; \qquad (2)$$

where k_{p_dc} and k_{i_dc} are equal to 0.3 and 0.001, respectively, v_{dc}* is the control reference signal of the DC-link voltage (Fig 1), e_{dc} corresponds to the dc-link voltage error, and $acum_{dc}$ comprehends the integral of the PI controller, being updated at each sampling period. These gains (k_{p_dc} and k_{i_dc}) were conceived through preliminary simulations and, moreover, the parameters of this controller were normalized. A phase-locked-loop (PLL) synchronizing circuit is applied to synchronize i_{cr} with the fundamental component of the grid voltage. Such PLL strategy is similar to that introduced by Elrayyah [16] and it yields signal v_{pll} in (2). It is well known that a common drawback among most of single-phase PLL circuits concerns the presence of an oscillating component at 2ω, which usually leads to the use of low-pass filters. In this work, the chosen PLL method eliminates the referred oscillating component and the need of low-pass filters. The periodic sampling technique is used to modulate the reference current i_{cr}*. Essentially, i_{cr}* is compared with the AC output current, i_{cr}, if one considers its direction as indicated in Fig 1. In this case, the AC output voltage of the active rectifier (v_{cr}) is equal to + v_{dc} when i_{cr}* is higher than i_{cr} and, otherwise, v_{cr} is equal to – v_{dc}.

B. PWM Inverter

The V/Hz speed controller conjoined with the sinusoidal PWM (SPWM) technique constitutes the control algorithm of the PWM inverter as exposed in Fig. 3. Two feedback loops, one for the mechanical speed N_m and other for the peak value of the fundamental voltages v_{ab}, v_{bc} and v_{ca}, can also be seen in this figure.

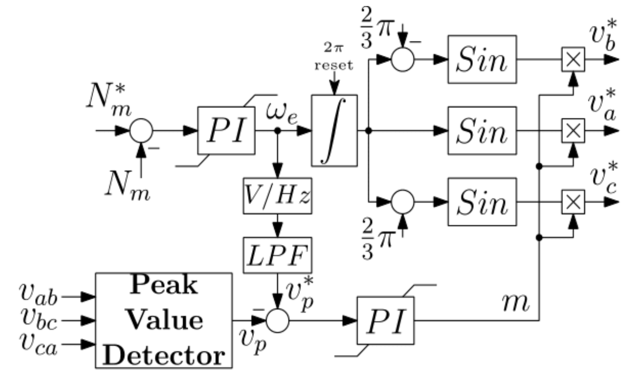

Figure 3. Control block diagram of PWM three-phase inverter: voltage regulation and power control (through speed control)

For the purpose of avoiding malfunction on the PI controllers, the one used to determine the electrical frequency, ω_e, must operate with lower dynamics than that of the other one used for generating the modulation index *m*, which corresponds to the normalized amplitude of the AC output voltages. The output signal of the V/Hz block (v_p*) is the reference signal of the modulation index PI controller, whereas the three-phase reference voltages are v_a*, v_b* and v_c*. The signal v_p* is compared to v_p which is the output of the Peak Value Detector (Fig 3). Assuming a low harmonic-distortion of the line voltages, v_p was calculated as follows:

$$v_p = \sqrt{\frac{2}{9}(v_{ab}^2 + v_{bc}^2 + v_{ca}^2)}\,. \tag{3}$$

By reason of possible presence of oscillating components on the mechanical speed, which may increase at transient occurrences, a low-pass filter (LPF) is placed at the output of the V/Hz block. Furthermore, one must note that the modulation index, *m*, is indirectly influenced by the DC-link voltage, which, on the other hand, is dynamically modified while the MPP is not achieved. Indeed, an increment or decrement on the DC-link voltage modifies the average value of v_p and, consequently, the PI controller settles a new value to *m* such that the error between v_p* and v_p is reduced to zero.

Based on preliminary simulations, the obtained proportional and integral gains of the PI controller to determine ω_e are equal to 2.0 and 0.8, respectively. On the other hand, the proportional and integral gains of the PI controller to determine the modulation index (*m*) are equal to 5.0 and 2.0, respectively.

C. Proposed MPPT Algorithm

Fundamentally, Maximum Power Point Tracking (MPPT) algorithms are applied to determine the set point, usually of voltage or active power, on which the renewable source produces its maximum energy. In this paper, the control reference variable is the DC-link voltage. Hence, the MPPT determines dynamically the reference value of the DC-link voltage, v_{dc}*, by forcing the PV string to produce its maximum energy, corresponding to the Maximum Power Point (MPP).

MPPT algorithms may achieve the MPP through online or offline methods [17]. Offline methods are based on a database for different values of irradiance and temperature where, for each combination of those data, there is only one control reference voltage corresponding to the MPP. Each combination of irradiance and temperature values with the corresponding set point (MPP) is used to establish approximation functions or correlations, such as those coming from fuzzy logic, linear regression and neural network based methods [18] that best track the MPP. An advantage is the possibility to reach the set point very fast. On the other hand, it may not lead to the real MPP.

Online methods are based on iterative algorithms to determine the set point, for instance the Perturb and Observe P&O algorithm, which is the most widely used one due to its simplicity of implementation. A drawback is the resulting oscillation around the MPP when the chosen step does not lead to the correct set point. Other MPPT approach is the Incremental Conductance (InC) method, whereby the step size may be variable or not [19]. Nevertheless, depending on the chosen limits (maximum and minimum) of the step size, it is susceptible to different convergence speeds and oscillations around MPP [20]. Other way to realize MPPT is by means of the Gradient Method (GM) [14]. In these works, auxiliary algorithms to dynamically adjust the step size for reaching the set point were included.

Differently from the aforementioned methods, the Extremum Seeking Controller (ESC) [21] based MPPT generates a signal composed of a DC component added to an AC high frequency component (chattering waveform). Such output signal is usually normalized and applied as duty-cycle for the PWM modulator of a DC-DC converter.

Dissimilarly, in this paper, the output signal of the proposed modified InC based MPPT strategy operates as reference voltage v_{dc}* in Fig. 1 for the DC-link voltage controller. Further explanations on the proposed method are given as follows.

By considering the power-voltage curves illustrated in Fig. 2, and assuming that for each curve all of the PV cells are submitted to the same temperature and irradiance conditions, it can be seen there is one and only one maximum point, which corresponds to the global maximum point. The proposed algorithm is an improved version of the InC method, whose classical form is expressed as:

$$\frac{\partial p}{\partial v} = \frac{i\,\partial v}{\partial v} + \frac{v\,\partial i}{\partial v} = i + v\frac{\partial i}{\partial v}\,; \tag{4}$$

where power, voltage and current are represented by *p*, *v* and *i*, respectively. Since the algorithm performs discrete time equations, the discretized form (4) is given as:

$$\frac{\partial p}{\partial v}[k] = i_{pv}[k] + v_{dc}[k]\,\frac{i_{pv}[k] - i_{pv}[k-1]}{v_{pv}[k] - v_{pv}[k-1]}\,; \tag{5}$$

being v_{dc} the output voltage of the pv string, which is the same voltage at the dc-link voltage of the back-to-back converters, and i_{pv} is the output current of the pv string. On the Maximum Power Point (MPP) the derivative function $\partial p / \partial v$ is equal to zero, which leads to the following condition:

$$\frac{i_{pv}[k]}{v_{dc}[k]} = -\frac{i_{pv}[k] - i_{pv}[k-1]}{v_{pv}[k] - v_{pv}[k-1]}\,. \tag{6}$$

While the MPP is not reached, the reference voltage to the dc-link is updated as follows:

$$\begin{cases} v_{dc}^*[k] = v_{dc}^*[k] + \delta,\ \ if\ (\partial p)/(\partial v) > 0 \\ v_{dc}^*[k] = v_{dc}^*[k] - \delta,\ \ if\ (\partial p)/(\partial v) < 0 \end{cases}; \tag{7}$$

being δ a positive integer.

One must note that this method is prone to low frequency noise once the MPP is achieved. Such oscillations can be caused by two factors as follows. The voltage and current sampling frequency is the same as that of the reference voltage updating procedure. Secondly, the use of a fixed constant, δ, to update the reference voltage, directly influences the time period necessary for the algorithm to converge to MPP. As a matter of fact, if δ is small, the system will converge to MPP with good precision but slowly. Otherwise, if δ is large, the convergence time to MPP is reduced, nevertheless precision is compromised.

Thence, in this work, the reference voltage updating procedure is done through variable frequency different from the sampling frequency as indicated in Fig. 4. The resulting

MPPT algorithm is enabled when the condition,

$$\left|\overline{v_{dc}}[j]-v_{dc}^{*}[n]\right|<\xi; \tag{8}$$

is fulfilled, where $\overline{v_{dc}}$ is the average value of the DC-link voltage; j is the sampling frequency for renewing it , n is the sampling frequency for renewing v_{dc}* and ξ is a constant that was determined through preliminary simulations. The average value of the DC-link voltage is obtained over 10,000 samples that correspond to 4Hz or 15 cycles of 60Hz. Essentially, the InC method is based on derivative equation and stability may be compromised in case of high-frequency component at the input signal. To overcome this drawback, a low-pass filter to extract the average component of v_{dc} was included. Once the algorithm is enabled to determine a new value of reference voltage and $G_1[n]$ is determined as follows:

$$G_1[n]=i_{pv}[n]+v_{dc}[n]\cdot\frac{(i_{pv}[n]-i_{pv}[n-1])}{(v_{DC}[n]-v_{DC}[n-1])}\quad. \tag{9}$$

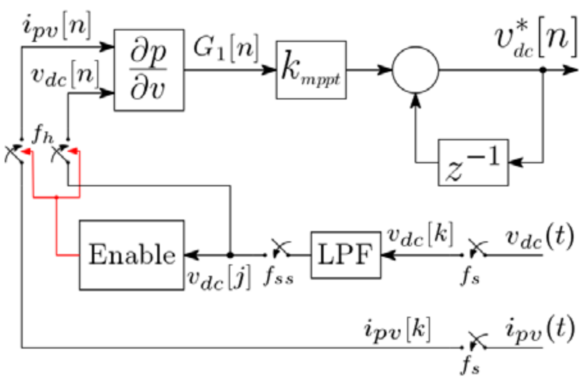

Figure 4. Block diagram of the proposed modified InC based MPPT algorithm

The k_{mppt} parameter is a constant equal to 0.2, and it was determined through preliminary results. It is important to note that the resulting increment is variable so that it increases or decreases in the same way as the difference between the current reference and the MPP varies, which corresponds to the principle of the *gradient descent method*. Thus, one can see a combination of two optimizing methods to conceive the proposed MPPT is this work. Hence, fast convergence with good precision at MPPT is possible. Moreover, the increment tends to zero when the reference is in vicinity of the MPP. Accordingly, no low-frequency component is present when the system is at steady-state operation with MPP. Furthermore, one must note that the proposed MPPT presents two constant sampling periods, k and j, and one variable sampling period (n), which is a multiple integer of j.

An example illustrating the performance of the proposed MPPT algorithm is shown in Fig.5, where Fig. 5(a) shows DC-link voltage tracking the reference value determined by the MPPT algorithm, while in Fig. 5(b) the corresponding active power of the PV string is presented.

It is worth mentioning that G_1 increases at MPP, once the voltage variation $v_{dc}[n]$ – $v_{dc}[n\text{-}1]$ is close to zero, what would make the system unstable. To overcome this problem, minimums values of 100 mV and 25W/V were set for the DC-Link voltage and $G_1[n]$, respectively.

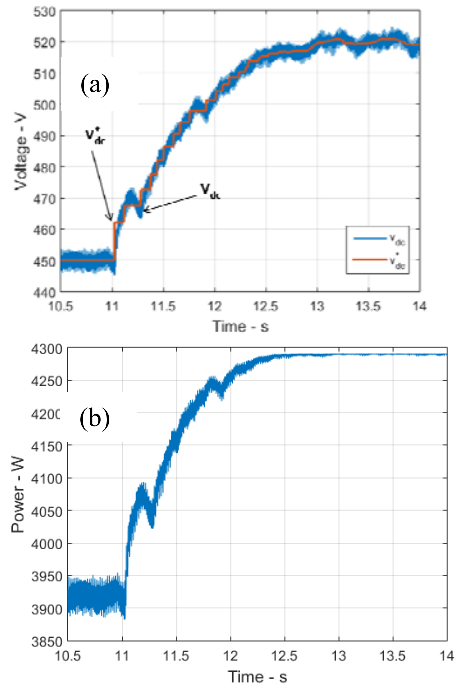

Figure 5. Performance of the proposed modified InC based MPPT algorithm, with (a) v_{dc}*[n] being updated when control block enable is activated, and (b) the corresponding active power of the PV string

IV. SIMULATION RESULTS

In this Section, simulation results to evaluate the performance of the proposed PV solar energy system (Fig. 1) are presented. The analysis is carried out with fixed time-step, total time and sampling frequency equal to 2 μs, 70 s, and 40 kHz, respectively. The test case analysis, as shown in Fig. 6 up to Fig. 10, starts with power converters turned off, all of the control algorithms disabled and motor at zero speed.

Fig. 6 illustrates the MPPT performance under transient and steady-state conditions. The irradiance (Fig. 6(a)) is maintained at 1 kW/m^2 and, just after t = 15s, it is gradually decreased by several steps down to 200 W/m^2, and, in sequence, is increased with these same steps up to 1 kW/m^2. The active rectifier and the DC-link voltage controllers are enabled at t = 100ms (Fig. 6(b)). Initially, the rectifier controller sets the DC-link voltage at 450 V, which is the threshold that assures its controllability.

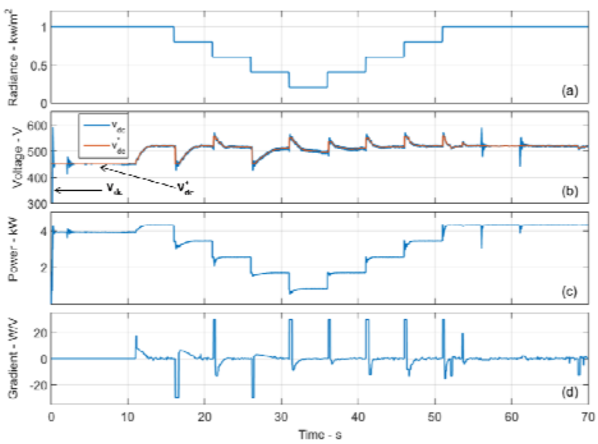

Figure 6. MPPT performance under transient and steady-state conditions. a) Irradiance; b) DC-Link voltage (v_{dc}, in blue) and its control reference (v_{dc}*, in orange); c) Power generated by the PV string; d) Gradient, $\partial P/\partial v$

At t = 11s, the MPPT algorithm is enabled and it makes the DC-link voltage (Fig. 6(b) and the PV string generated power (Fig. 6(c)) be built up to the optimum set point, as indicated by the variable labeled "Gradient" (Fig. 6(d)). This variable corresponds to $\partial p/\partial v$ expressed in (5) and, therefore, the MPP is reached when the average value of "Gradient" is equal to zero. In Fig. 6(d), one can see that MPP is achieved at each transient event.

It is important to highlight the capability to extract the maximum energy from the PV string even at low irradiance levels (200W/m^2). In southeast region of Brazil, low irradiance typically occurs around 7 a.m. and 6 p.m. Thus, system operation during more than 10 hours is possible. Furthermore and predictably, the DC-link voltage does not present low-frequency oscillations around the MPP at steady-state condition.

Fig. 7 illustrates the motor performance with the implemented system controller. The motor controller starts the motor at t = 2s, and increases the rotor speed up to 1719 rpm in a ramp-shaped pattern until t = 10s (Fig. 7(a)). The motor is kept at constant speed from t = 10s until t = 56s. As can be seen in Fig. 7(a), the motor is able to track the ramp-shaped speed reference (N_m*, in orange color) without any overshoot in marked contrast to the results in [14]. Besides, the system performs step changes of speed with short-time transients and negligible overshoot. One can see that during the simulation period, the solar irradiance (Fig. 6(a)) was modified to evaluate the MPPT performance under constant load. After t = 56s, the irradiance is constant while the motor speed is reduced down to 1000 rpm, and at t = 62s it is increased to its rated value of 1719 rpm (Fig. 7(a)). Since the motor is driving a fan-type load, the speed change leads to a load change, and this establishes the scenario for performance analysis of the proposed MPPT under variable load conditions. Fig. 7(b) presents the modulation index variations during the time interval in which the speed is constant. These variations are on account of the DC-link voltage behavior that follows the MPPT impositions to reach the optimal set point (MPP) of the PV string. The mechanical torque and the active and reactive powers drawn by the motor are shown in Fig. 7(c) and Fig. 7(d), respectively. As expected, the voltage control loop of the V/Hz control has slower response than that of its speed control loop.

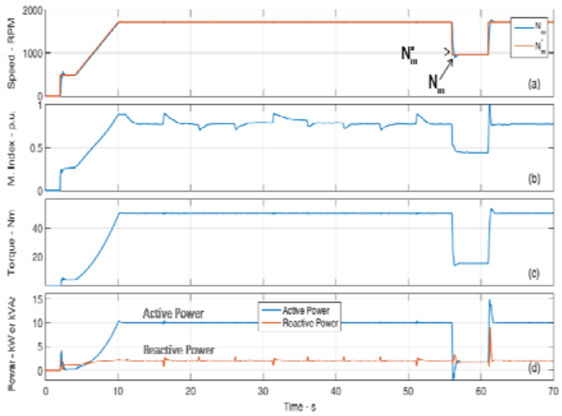

Figure 7. Motor performance with the implemented speed controller. a) Speed (N_m) and its control reference N_m*; b) Inverter modulation index; c) Mechanical Torque; d) Active (in blue) and Reactive Power (in orange) drawn by motor

Fig. 8(a) presents the active power drawn by the active rectifier and the corresponding grid current (i_S) is illustrated in Fig. 8(b). This active power means the difference between the generated active power by the PV string and the consumed active power by the motor load. It is worth noting that the PV string (Fig. 6(c)) minimizes the active power drawn by the active rectifier when the irradiance is higher than 800W/m2 (Fig. 6(a)).

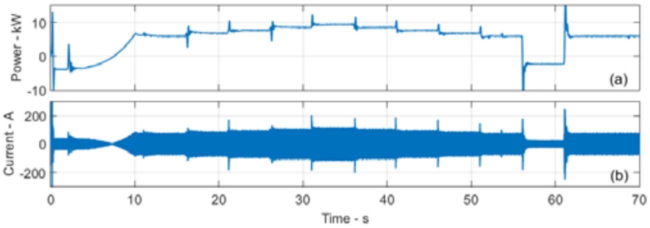

Figure 8. Grid-side variables during the entire simulation; a) Active power of the AC single-phase circuit; b) Rectifier Current, i_S.

Grid voltage, v_f, and current, i_S, during motor speed transition from 1719 rpm down to 1000 rpm are shown in Fig. 9. At this transient interval, the PV string active power is more than 4 kW (Fig. 6(c)) and, due to the speed controller action, the active power drawn by the motor is also reduced from 10 kW to 2 kW (Fig. 7(d)). In this case, the excess energy generated by the PV string goes to the single-phase grid and i_S is in counter-phase with v_f, as shown in Fig. 9. It can be seen that low-frequency oscillations occur on current i_S. It occurs because of the dynamics of DC-link voltage and speed motor controllers. This interaction effect makes i_S reach a novel steady-state condition at t = 58s (Fig. 8(b)).

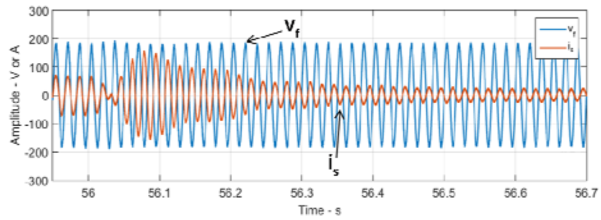

Figure 9. Grid voltage and grid-side converter current during the transient when the motor speed decreases from 1719 rpm to 1000 rpm

In Fig. 10, the grid-side voltage v_f and current i_S are presented during the last transient motor-speed event (Fig. 7(a)), wherein it is stepped up from 1000 rpm to 1719 rpm. Accordingly, the active power drawn by the motor rises from 2 kW up to 10 kW (Fig. 7(d)), while the PV string active power is more than 4 kW (Fig. 6(c)). In this case the complementary energy necessary to supply the motor is provided by the single-phase grid, and i_S becomes in phase with v_f. Similarly to Fig. 9, low-frequency oscillations are there in Fig. 10, until the steady-state condition is achieved at t = 64s.

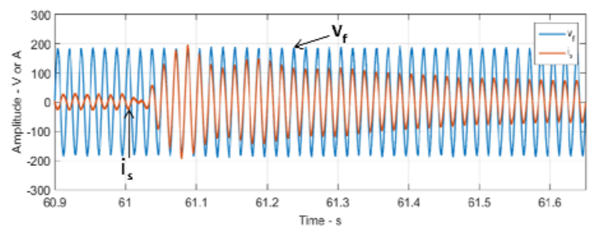

Figure 10. Grid voltage and grid-side converter current during the transient when the motor speed increases from 1000 rpm to 1719 rpm

An overall performance of the grid-tied PV generation system, during a 35% voltage sag at the single-phase grid, while the solar irradiance is very low at 200W/m^2, is illustrated in Fig. 11, where Fig. 11(a) and Fig. 11(c) are the waveforms of the voltage and current at the single-phase grid. In this test case the objective was to identify the maximum voltage sag that the hybrid generation system is able to withstand, considering the lowest solar irradiance with the load active power at its nominal value of 10 kW.

One can see that the DC-link (Fig. 11(b)) is able to track the control reference settled by the MPPT algorithm (orange line), and the PV string power (Fig. 11(d)) is maintained at the expected 800 W. The ride-through capability at voltage sags higher than 35% will improve with increasing irradiance.

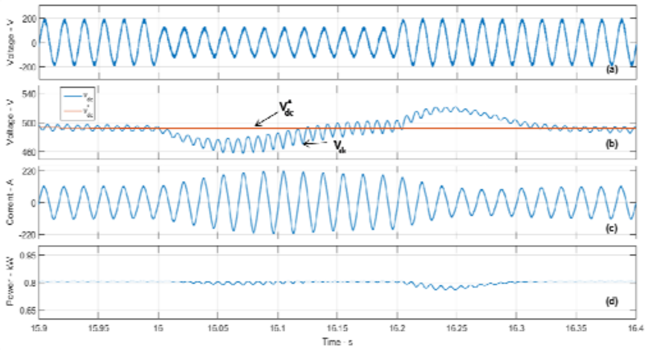

Figure 11. Overall performance of the grid-tied PV generation system in case of voltage sag at the single-phase grid, with a solar irradiance of 200W/m^2. (a) Rectifier AC voltage, (b) DC-link voltage and the reference dc-link voltage determined by the MPPT controller (orange), (c) Rectifier AC current, (d) produced active power by the PV strings

A. *Summary of Results*

Some results are summarized in Table 1 and Table 2. Table 1 shows that simulated MPP test cases match those theoretical results obtained from the PV curves of Fig. 2, evaluating the effectiveness of the proposed MPPT algorithm to achieve the optimum set point under different load and irradiance conditions. Finally, Table 2 presents the values of Total Harmonic Distortion (THD %) of the grid current (i_S) in relation with the irradiance and the motor speed. As expected, the THD% increases as the rms grid current goes down, since it is related with the fundamental component of i_S. Nevertheless, even at worst case scenario, the THD% is not higher than 5%, which is acceptable based on IEEE recommendations [22].

TABLE I. COMPARISON BETWEEN MPP OBTAINED THROUGH THE PROPOSED MPPT AND WITH THE THEORETICAL RESULTS

Irradiance (W/m^2)	**MPP (kW)**	
	Theoretical	**Proposed MPPT**
1000	4.23	4.23
800	3.38	3.38
600	2.52	2.52
400	1.66	1.66
200	0.81	0.81

TABLE II. TOTAL HARMONIC DISTORTION OF THE RECTIFIER CURRENT IN RELATION TO THE IRRADIANCE AT CONSTANT MOTOR SPEED OF 1719 RPM

Irrandiance (W/m^2)	**THD of the Rectifier Current (%)**
1000	5.0
800	4.8
600	4.8
400	4.7
200	4.9

B. *Economic Feasibility Study*

Another important issue to assess the practicality of a proposed system project is its economic feasibility. Thus, a case study to estimate the energy and time period payback related with the investment to implement an experimental prototype of the studied system is presented in this section. To develop this economic study the following aspects were taken into account: *i*) the electricity tax-rates per kWh practiced by the Brazilian utility companies in rural areas; *ii*) the energy production resulting from the average solar irradiance in southeast region of Brazil over a period of one year; *iii*) and the costs involving all of the electronic components considered for the project.

Table 3 summarizes the costs to build the proposed prototype, based on the specifications denoted in Section 2 and the corresponding price quotations done by the time this system was studied. Microcontrollers, hall-effect sensors and other electronic devices were labeled as instrumentation and control circuitry in Table 3. Table 4 indicates the payback period of the investment to build the prototype, considering the energy produced by 17 solar PV panels as specified in Section 2, over a period of one year.

Upon initial inspection of Table 3 results, it may lead to the conclusion that more than 15 years are necessary to recover these investments. Nevertheless, other aspects that may shorten the payback time period, and are difficult to express mathematically, must be considered such as, the improvement of power quality and of the overall drive system reliability under sudden AC grid voltage variations, and consequent increase of equipment service life. Other important issue is the technological advances in semiconductor films resulting in more efficient PV panels at lower costs. Hence, by looking upon these considerations, one can see the probability of the determined energy payback period to considerably be reduced in the near future, which is feasible due to the higher demand of renewable energy sources, particularly in rural or remote areas [23]. Additionally, the capital costs described in Table 3 clearly suggest that a system with part-count reduction may result economically advantageous, though detailed performance analysis is required for a final engineering decision. In this Case, VA ratings and energy losses in power components must come into consideration.

TABLE III. CAPITAL COSTS

Item	**Capital Costs ($USD)**
Solar Panels	3,500
Power Converters	3,500
Three-Phase Transformer and Passive Elements	2,000
Instrumentation & Control Circuitry	500,00
TOTAL	**9,500**

TABLE IV. PAYBACK OF THE INVESTMENT

Electricity tax rate	0.15 ($USD/kWh)
Energy Production	4.304 (MWh/year)
Payback of the Investment	**645.69 ($USD/year)**

V. CONCLUSIONS

This paper has presented the design guidelines and performance analysis, and economic feasibility study as well, of a grid-tied PV generation system. The studied configuration has been based on a single-phase to three-phase system built up with conventional five-leg full-bridge converter with output transformer.

A PV string has been connected to the DC-link dispensing with the need for an extra converter to perform MPPT. A MPPT controller founded on a modified InC method, with the ability to minimize low-frequency oscillations around the MPP, and capable to track the MPP even under disturbances at the DC-link voltage, has been proposed. The system has supplied an induction motor coupled to a fan-type load, and has been tested under single-phase AC mains voltage sag, and different load and irradiance conditions.

Simulation results have shown the effectiveness of the proposed energy system management to deliver energy either to the load or to the grid, with the PV string producing its maximum energy even under different transient events. It follows that the studied system is economically feasible and possesses attractive features for rural grid applications and for other weak power-grids, such as, islanded grids. The authors believe that the work presented here will be helpful for future research on converter topologies and control algorithms applied for renewable energy systems.

REFERENCES

[1] B. K. Bose, "Global energy scenario and impact of power electronics in 21st century," IEEE Transactions on Industrial Electronics, vol. 60, no. 7, pp. 2638-2651, 2013, doi:10.1109/TIE.2012.2203771.

[2] M. Z. Jacobson and M. A. Delucchi, "A path to sustainable energy by 2030," Scientific American, vol. 301, no. 5, p. 58-65, 2009, doi:10.1038/scientificamerican1109-58.

[3] J. M. Guerrero *et al.*, "Distributed Generation: Toward a New Energy Paradigm," IEEE Industrial Electronics Magazine, vol. 4, no. 1, pp. 52-64, 2010, doi:10.1109/MIE.2010.935862.

[4] D. Debnath and K. Chatterjee, "Solar photovoltaic-based stand-alone scheme incorporating a new boost inverter," IET Power Electronics, vol. 9, no. 4, pp. 621-630, 2016, doi:10.1049/iet-pel.2015.0112.

[5] M. Liserre *et al.*, "The Smart Transformer: Impact on the Electric Grid and Technology Challenges," IEEE Industrial Electronics Magazine, vol. 10, no. 2, pp. 46-58, June 2016, doi:10.1109/MIE.2016.2551418.

[6] J. Marsden, "Distributed Generation Systems: A New Paradigm for Sustainable Energy," IEEE Green Technologies Conference, Baton Rouge, LA, USA, 2011, pp. 1-4, doi:10.1109/GREEN.2011.5754858.

[7] S. Kouro, J. L. Leon, D. Vinnikov, L. G. Franquelo, "Grid-Connected Photovoltaic Systems: An Overview of Recent Research and Emerging PV Converter Technology," IEEE Industrial Electronics Magazine, vol. 9, no. 1, pp. 47-61, 2015, doi:10.1109/MIE.2014.2376976.

[8] P. Wolfs and F. Yang, "A single to three phase power converter with integrated storage and a PV interface for rural power applications," 2014 IEEE PES General Meeting | Conference & Exposition, National Harbor, MD, USA, pp. 1-5, 2014, doi:10.1109/PESGM.2014.6938833.

[9] R. K. Behera and O. Ojo, "Modeling and control of DAB converter for solar micro-grid application," 6th International Conference on Power Electronics Systems and Applications (PESA), Hong Kong, pp. 1-5, 2015, doi:10.1109/PESA.2015.7398899.

[10] R. Z. Scapini, C. Rech, T. B. Marchesan, L. Schuch, R. F. de Camargo and L. Michels, "Capability Analysis of a D-STATCOM Integrated to a Single-Phase to Three-Phase Converter for Rural Grids," IEEE 23rd International Symposium on Industrial Electronics (ISIE 2014), Istanbul, Turkey, pp. 2560-2565, 2014. doi:10.1109/ISIE.2014.6865023.

[11] R. Q. Machado, S. Buso and J. A. Pomilio, "A Line-Interactive Single-Phase to Three-Phase Converter System," IEEE Transactions on Power Electronics, vol. 21, no. 6, pp. 1628-1636, 2006, doi:10.1109/TPEL.2006.882963.

[12] E. C. D. Santos, C. B. Jacobina, N. Rocha, J. A. A. Dias and M. B. R. Correa, "Single-phase to three-phase four-leg converter applied to distributed generation system," IET Power Electronics, vol. 3, no. 6, pp. 892-903, 2010, doi:10.1049/iet-pel.2009.0240.

[13] N. Rocha, Í. A. C. de Oliveira, E. C. Menezes, C. B. Jacobina and J. A. A. Dias, "Single-Phase to Three-Phase Converters With Two Parallel Single-Phase Rectifiers and Reduced Switch Count," IEEE Transactions on Power Electronics, vol. 31, no. 5, pp. 3704-3716, 2016, doi:10.1109/TPEL.2015.2458699.

[14] E. A. Rodriguez, C. M. Freitas, M. D. Bellar and L. F. C. Monteiro, "MPPT algorithm for PV array connected to a Hybrid Generation System," IEEE 24th International Symposium on Industrial Electronics, (ISIE 2015), Búzios, Brazil, pp. 1115-1120, 2015, doi:10.1109/ISIE.2015.7281628.

[15] Â. Araújo, J. G. Pinto, B. Exposto, C. Couto and J. L. Afonso, "Implementation and comparison of different switching techniques for shunt active power filters," IEEE 40th Annual Conference of the Industrial Electronics Society (IECON 2014), Dallas, USA, pp. 1519-1525, 2014, doi:10.1109/IECON.2014.7048703.

[16] A. Elrayyah, Y. Sozer and M. Elbuluk, "Robust phase locked-loop algorithm for single-phase utility-interactive inverters," IET Power Electronics, vol. 7, no. 5, pp. 1064-1072, 2014, doi:10.1049/iet-pel.2013.0351.

[17] M. A. G. de Brito *et al*., "Evaluation of the Main MPPT Techniques for Photovoltaic Applications," IEEE Transactions on Industrial Electronics, vol. 60, no. 3, pp. 1156-1167, 2013, doi:10.1109/TIE.2012.2198036.

[18] K. Rouzbehi, A. Miranian, A. Luna and P. Rodriguez, "Identification and maximum power point tracking of photovoltaic generation by a local neuro-fuzzy model," IEEE 38th Annual Conference on Industrial Electronics Society (IECON 2012), Montreal, Canada, pp. 1019-1024, 2012, doi:10.1109/IECON.2012.6388581.

[19] D. Lalili, A. Mellit, N. Lourci, B. Medjahed and E. Berkouk, "Input output feedback linearization control and variable step size MPPT algorithm of a grid-connected photovoltaic inverter," Renewable energy, vol. 36, no. 12, pp. 3282-3291, 2011, doi:10.1016/j.renene.2011.04.027.

[20] R. Faraji *et al*., "FPGA-based real time incremental conductance maximum power point tracking controller for photovoltaic systems," IET Power Electronics, vol. 7, no. 5, pp. 1294-1304, 2014, doi:10.1049/iet-pel.2013.0603.

[21] I. Munteanu and A. Bratcu, "MPPT for grid-connected photovoltaic systems using ripple-based Extremum Seeking Control: Analysis and control design issues," Solar Energy, vol. 111, pp. 30-42, 2015, doi:10.1016/j.solener.2014.10.027.

[22] IEEE recommended practice and requirements for harmonic control in electric power systems, IEEE Std 519-2014 (Revision of IEEE Std 519- 1992), 2014, doi:10.1109/IEEESTD.2014.6826459.

[23] A. Zomers, "Remote Access: Context, Challenges, and Obstacles in Rural Electrification," IEEE Power and Energy Magazine, vol. 12, no. 4, pp. 26-34, 2014, doi:10.1109/MPE.2014.2315916.